Flexural strength and fatigue properties of interfacial transition zone at the microscale

Gan, Yidong; Zhang, Hongzhi; Liang, Minfei; Zhang, Yu; Schlangen, Erik; van Breugel, Klaas; Šavija, Branko

DOI
10.1016/j.cemconcomp.2022.104717

Publication date
2022

Document Version
Final published version

Published in
Cement and Concrete Composites

Citation (APA)
Gan, Y., Zhang, H., Liang, M., Zhang, Y., Schlangen, E., van Breugel, K., & Šavija, B. (2022). Flexural strength and fatigue properties of interfacial transition zone at the microscale. *Cement and Concrete Composites*, *133*, Article 104717. https://doi.org/10.1016/j.cemconcomp.2022.104717

Cement and Concrete Composites 133 (2022) 104717

Contents lists available at ScienceDirect

Cement and Concrete Composites

journal homepage: www.elsevier.com/locate/cemconcomp

Flexural strength and fatigue properties of interfacial transition zone at the microscale

Yidong Gan [a], Hongzhi Zhang [b,c], Minfei Liang [a,*], Yu Zhang [a], Erik Schlangen [a], Klaas van Breugel [a], Branko Šavija [a]

[a] Microlab, Faculty of Civil Engineering and Geosciences, Delft University of Technology, Delft, 2628, CN, the Netherlands
[b] School of Qilu Transportation, Shandong University, Jinan, PR China
[c] Suzhou Research Institute, Shandong University, Suzhou, PR China

ARTICLE INFO

Keywords:
Flexural strength
Fatigue
Microscale testing
Interfacial transition zone

ABSTRACT

In this study, the flexural strength and fatigue properties of interfacial transition zone (ITZ) were experimentally investigated at the micrometre length scale. The hardened cement paste cantilevers (150 × 150 × 750 μm^3) attached to a quartzite aggregate surface were prepared and tested under the monotonic and cyclic load using a nanoindenter. The measured flexural strength of the ITZ (10.49–14.15 MPa) is found to be one order of magnitude higher than the macroscopic strength of ITZ reported in literature. On the other hand, the fatigue strength of the ITZ is lower than that of bulk cement paste at same length scale, measured previously by the authors. The microscopic mechanical interlocking and the electrostatic interaction between aggregate surface and hydration products are thought to contribute to the bond strength of ITZ. This study provides an experimental basis for the development of multiscale analysis of concrete subjected to both static and fatigue loading.

1. Introduction

The phenomenon of concrete fracture subjected to the monotonic and cyclic loading is very complex as it inherently involves multiple spatial scales owing to the multiscale heterogeneous nature of concrete [1,2]. At the mesoscale (millimeter to centimeter scale), concrete is generally considered as a three-phase composite comprising aggregate, cement paste matrix and the interfacial transition zone (ITZ) – a highly porous zone between the aggregate particles and the cement paste matrix. The ITZ plays an important role in the mechanical performance of concrete. To address the essential question of how the fracture process happening at smaller scales affects the macroscopic performance of concrete, experimental investigations combined with simulations are needed at every scale. Moreover, it has been reported that the strength, fatigue crack growth rate and fatigue life of cement-based materials, e.g. cement paste and concrete, exhibit a strong size effect [3–6]. A concrete specimen with a smaller geometric size generally shows a higher strength and better fatigue resistance for a given stress magnitude. However, the possible size-dependent mechanical and fatigue properties of ITZ have never been examined so far. Therefore, more experimental investigations are needed on this aspect. Over the past decades, numerous studies have been performed to investigate the microstructure development and the mechanical properties of ITZ [7–12]. The ITZ is generally characterized by high porosity, deposition of crystals with preferential orientations and fewer cement particles than in the bulk cement matrix. The major origin of this porous ITZ is due to the so-called 'wall effect', which disrupts the packing of the cement grains against the relatively flat aggregate surface [7]. Moreover, a water film which forms around aggregate particles in fresh concrete also leads to a higher local w/c ratio in the vicinity of aggregate particles. Another important microstructural feature of ITZ is the excess content of large ettringite (AFt) and calcium hydroxide (CH) crystals with preferential orientations deposited in the vicinity of aggregate, which forms the porous framework of ITZ at the early age of hydration [12]. With ongoing hydration, the remaining space is further filled with calcium silicate hydrate (C–S–H) gel and smaller crystals of AFt and CH.

In general, the porous ITZ is considered to be the weakest link in conventional concretes and is prone to microcracking under loading. To characterise the mechanical properties of ITZ at different scales, various testing approaches have been developed in literature [7–13]. While

* Corresponding author.
E-mail addresses: y.gan@tudelft.nl (Y. Gan), hzzhang@sdu.edu.cn (H. Zhang), M.Liang-1@tudelft.nl (M. Liang), Y.Zhang-28@tudelft.nl (Y. Zhang), Erik.Schlangen@tudelft.nl (E. Schlangen), K.vanBreugel@tudelft.nl (K. van Breugel), B.Savija@tudelft.nl (B. Šavija).

https://doi.org/10.1016/j.cemconcomp.2022.104717
Received 28 July 2021; Received in revised form 9 May 2022; Accepted 5 August 2022
Available online 10 August 2022

most studies focus on the macroscopic behaviour of ITZ due to technical and instrumental limitations, the typical thickness of ITZ (20–100 μm) is at the microscale. The recent applications of indentation techniques provide valuable information on the hardness and indentation modulus of ITZ [14,15]. Unfortunately, the strength of ITZ cannot be directly measured by the conventional indentation techniques. This can be overcome by fabricating small cement paste cantilevers attached on the aggregate and performing bending tests with the aid of a nanoindenter, as described in Ref. [16]. Zhang et al. [16] performed micro-bending tests on small ITZ cantilever beams with the dimension of 200 × 100 × 100 μm^3. The measured load-displacement curves were then used to calibrate and validate the micromechanical model and set basis for the multiscale modelling of mortar. In current study, the previously developed method is adjusted by increasing the size of specimen to 750 × 150 × 150 μm^3, which allows for the direct measurement of flexural strength of ITZ with negligible shear effect.

Unlike the static mechanical properties, the fatigue properties of ITZ have never been directly examined *at any length scale*. It is known that the fatigue-induced damage may severely affect the macroscopic mechanical of concrete [5,17,18]. The fatigue loading could also accelerate most of unavoidable ageing phenomena resulting in a decay of quality and function of system with elapsed time [19]. Therefore, a clear understanding of fatigue behaviour of ITZ is of great importance for predicting the fatigue of concrete structure. In the previous fatigue tests of cement paste at the microscale [5], the stiffness degradation of cement paste was very limited even subjected to a large number of cycles. However, the fatigue damage accumulation in concrete is more noticeable [20,21]. This may indicate that most of the fatigue damage occurs in the ITZ. It seems possible that the pre-existing cracks and pores situated in the ITZ would promote the development of fatigue cracks in concrete when subjected to cyclic loading [20,21].

Regarding the methods for fatigue analysis, there are roughly four categories in literature, i.e. the *S–N* curve based on experimental results [5,22], the linear elastic fracture mechanics based Paris' law for describing the fatigue crack propagation [23], the cohesive crack model based on the non-linear stress-crack width relationship [24] and the fatigue damage evolution model based on damage mechanics [25]. It is well known that fatigue of materials can be characterized by an *S–N* curve (stress level versus fatigue life), also known as the Wöhler curve [26]. If *N* is plotted in a logarithmic scale and *S* keeps in a linear scale, the *S–N* curve will become approximately a straight line. The experimentally obtained *S–N* curves are widely adopted and remain the primary design tool for predicting the fatigue life of concrete structures. In addition, the Paris' law is usually used to describe the crack growth rate under cyclic loading [23]. It states that the crack growth increment per load cycle can be defined as a function of the stress intensity factor range. The Paris' law and its modifications have also gained wide acceptance for the application in cementitious materials [4,27]. To consider the non-linear behaviour of fracture process zone ahead of crack tip, cohesive crack models based on measured or assumed stress-crack width relationships were developed [24]. An appealing feature of this approach is that the analytical expression can be easily implemented as a mathematical subroutine in numerical simulations. Since materials subjected to fatigue loading always experience progressive degradation of mechanical properties, damage mechanics has been extensively used to model the fatigue damage evolution in concrete [28–31]. In this approach, constitutive equations for damage evolution of damage variables are formulated in the framework of thermodynamics and calibrated with experimental data to model different damage processes.

This paper aims to study for the first time the flexural strength and fatigue properties of ITZ at the microscale. The miniatured ITZ specimens were first fabricated using a method similar to that developed by Zhang et al. [16]. The specimens were then subjected to both monotonic and cyclic loading to assess their flexural strength and fatigue properties, respectively. The *S–N* curves of ITZ specimens with different w/c ratios were established. The microscopic observations on the fracture surfaces were also performed to gain a better understanding of the ITZ fracture under different loading conditions. The possible size effect of ITZ bonding strength is examined by comparing with the macroscopic test results reported in the literature. Discussions on the origin of ITZ bonding strength and the fatigue behaviours of ITZ at the microscale were also provided.

2. Experimental methodology

2.1. Materials and sample preparation

Standard grade CEM I 42.5 N Portland cement (ENCI, the Netherlands) was mixed with deionized water to prepare the cement pastes. Two w/c ratios (0.3 and 0.4) were used in this study. The Blaine fineness of cement (provided by the manufacturer) is 2840 cm^2/g. Before the sample preparation, a chemically inert quartzite aggregate was cut and ground to obtain a thin slice with the thickness of 1 mm, see Fig. 1(a). This was achieved by using a Minitom low-speed cutting machine and a Struers Labopol-5 thin sectioning machine, respectively. Both sides of aggregate were ground using two grinding discs with grit sizes of 135 μm and 35 μm in sequence. Each grinding step lasted for about 5 min. The prepared aggregate slices were then dried in an oven (60 °C) for 48 h. The surface texture of the aggregate is an important factor affecting the mechanical properties of ITZ [10,32,33]. By means of mechanical interlocking with the aggregate surface at different length scales, the bonding strength of ITZ is higher for rough surface compared to smooth surface [11]. The microscopic mechanical interlocking is mainly caused by the epitaxial growth of cement hydration products (mostly CH and AFt) on the aggregate surface. The surface roughness of the ground aggregate was examined using a digital microscope (Keyence VHX-7000) with a z-axis resolution of 1 μm. The 3D contour map of surface roughness is shown in Fig. 1(b). Note that the height is calculated using an averaging technique in between two focal lengths. Two areas of 1000 × 1500 μm^2 were examined and the arithmetic mean height (S_a) and the root mean square height (S_q) are calculated as 4.5 ± 0.1 μm and 5.6 ± 0.1 μm. Clearly, the measured roughness in this study is much lower than (almost 1 to 3 orders of magnitude) the surfaces of nature aggregate and crushed aggregate reported in literature [34,35] but similar to the ground and polished aggregates [13]. In addition, the surfaces of slices were examined by using backscattered electron (BSE) images, secondary electron (SE) images and energy dispersive spectrometer (EDS) analysis, see Fig. 1(c) and (d). The accelerating voltage for EDS was chosen at 15 kV. It is confirmed from EDS analysis that the used aggregate mainly contains silica. Therefore, the chemical bonding is not the major source of the bonding strength between the cement paste and aggregate surface in the prepared ITZ sample. However, the electrostatic attraction between solid surfaces could possibly play a role, which will be further discussed in Section 3.3. Moreover, it can be seen from SE images of aggregate that the typical crystal size of quartz used in current study is around 7–15 μm.

The next step is to cast the mixed fresh cement pastes on the top surface of aggregate slice. Note that the casting procedure also affects the formation of ITZ [36]. The slice needs to be placed at the bottom of the plastic mold in order to avoid possible micro-bleeding effect [37]. The prepared samples were then cured under sealed conditions at room temperature for 28 days. After curing, the hydration of samples was arrested by solvent exchange method using the isopropanol. In order to accelerate water-solvent exchange, samples were repeatedly immerged five times and taken out for a period of 1 min.

For the fabrication of micro-cantilever beams containing the ITZ, a precision micro-dicing machine (MicroAce Series 3 Dicing Saw) equipped with a resin blade was used. To meet the limited cutting depth of this machine, the hardened cement paste-aggregate samples were further ground to reach the total thickness of around 1.75 mm (with approximately 1.00 mm aggregate + 0.75 mm cement paste). For more details

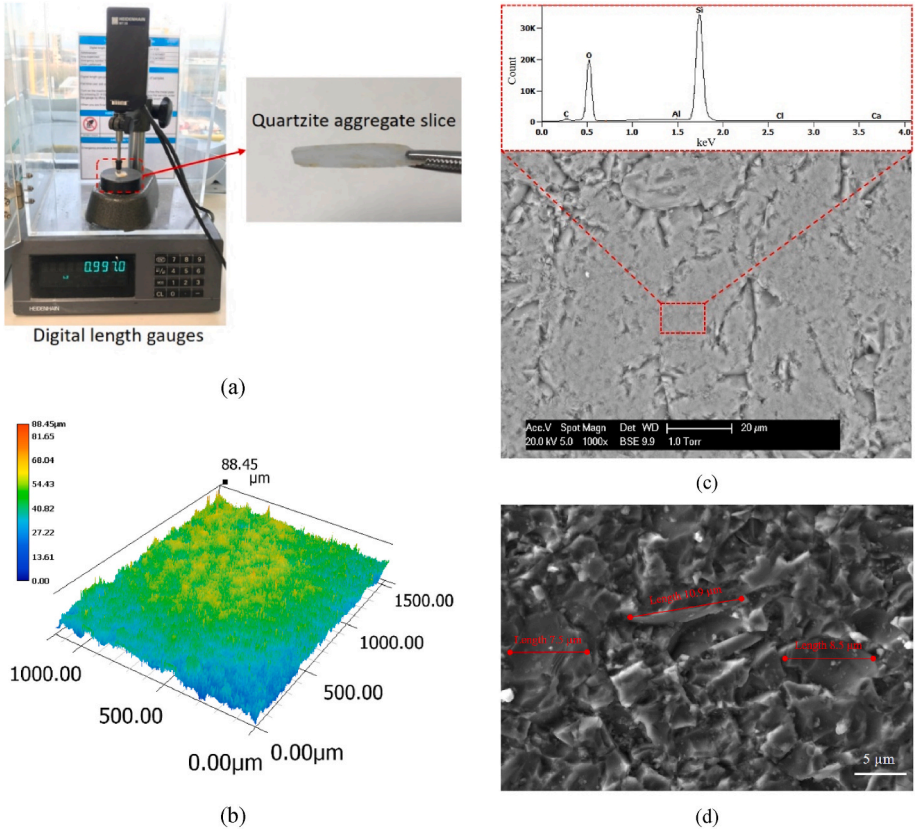

Fig. 1. (a) A slice of quartzite aggregate with the thickness of around 1 mm; (b) 3D contour map of suface roughness; (c) BSE image and EDS of aggregate surface and (d) SE image of quartz crystals.

regarding the sample preparation, the readers are referred to Ref. [16]. Only a brief description is given here: two perpendicular cutting directions with the same cutting spacing were applied on the cement paste side of sample using the micro-dicing machine. In this way, multiple rows of cement paste cantilever beams with a square cross section of the beam of 150 × 150 μm^2, which are attached on the aggregate surface, were fabricated. The cutting depth was set to 0.85 mm to ensure that the resin blade has cut into the aggregate. Hence, a clear boundary between the cement paste beam and the aggregate was generated, see Fig. 2(a). The resin blade may experience some attrition and damage with time especially when cutting into the stiff aggregate, which may undermine the quality of cutting. In this case, the replacement of new resin blade is required.

Note that the number of successfully prepared ITZ bond specimens is relatively low in comparison to that of pure cement paste specimen fabrication [5,16,17,38,39]. In other words, some cantilever specimens break during fabrication. This is mainly because that the ITZ is more heterogeneous than the bulk paste and tends to exhibit a larger variation of bond strength, which is in general much lower than the average strength of bulk paste. Since the ITZ bond specimens will inevitably experience some minor damage and shrinkage during the grinding and cutting procedure, the ITZ beam may be damaged or even fail before testing due to the high local porosity or the presence of shrinkage-induced cracks. Nevertheless, in successfully fabricated ITZ beams, no apparent cracking has been observed in cement paste beam or ITZ region as a consequence of the cutting process. An overall accuracy of the cross-sectional dimensions of ±2 μm can be reached with this fabrication process. The distance between the free end of cement paste and the edge of aggregate surface is defined as the effective cantilever length. In general, it is difficult to obtain a perfect flat and smooth surface of aggregate with the employed manual grinding procedure such that a slightly inclined aggregate surface is obtained, see Fig. 1(b). This results in some differences in effective cantilever lengths between samples. Nevertheless, the lengths of all samples were measured and recorded under the in-situ microscope before testing. Even though precautions have been taken to minimize the carbonation of the samples by storing the beams in isopropanol [40], the surfaces of miniaturized cement paste beams are inevitably carbonated when exposed to the ambient air, as can be seen in Fig. 2. Moreover, a relative rough boundary between the cement paste and aggregate can be observed at the higher magnification, see Fig. 2(a). This relative rough surface at the smaller scale along with the surface carbonation effect could potentially enhance the mechanical interlocking behaviour of ITZ to a certain extent [41].

The microstructures of four generated ITZ samples were examined using X-ray computed tomography (XCT) [42]. The X-ray source tube was set at 90 kV/170 μA during scanning, resulting in a voxel resolution of 0.5 × 0.5 × 0.5 μm^3. After acquiring the grey-value based XCT images, pore segmentation was conducted using the global threshold method [43,44]. The segmented XCT images were used to determine the porosity distribution along the beam. In Fig. 3, it is clear that the local porosity near the aggregate surface is larger than that of bulk paste [16]. The average porosity of the bulk paste, which is around 150 μm away from the edge of aggregate surface, is detected as 5.31 ± 1.08% for two w/c 0.3 samples. For two w/c 0.4 samples, the average porosity of bulk paste is 8.42 ± 1.63%. Note that pores smaller than the image resolution in XCT (i.e. 0.5 μm) cannot be detected. Therefore, a lower porosity is detected using the XCT compared to the mercury intrusion porosimetry method [45]. It is generally accepted that the ITZ is not a definite zone, but a region of transition. In the literature, the microstructure of ITZ is found to vary with the mix composition, hydration degree and casting procedure, etc [7,36]. Moreover, the local ITZ microstructures around one aggregate particle can significantly differ even in the same concrete sample [7]. Due to the ambiguous boundary with the bulk paste, it

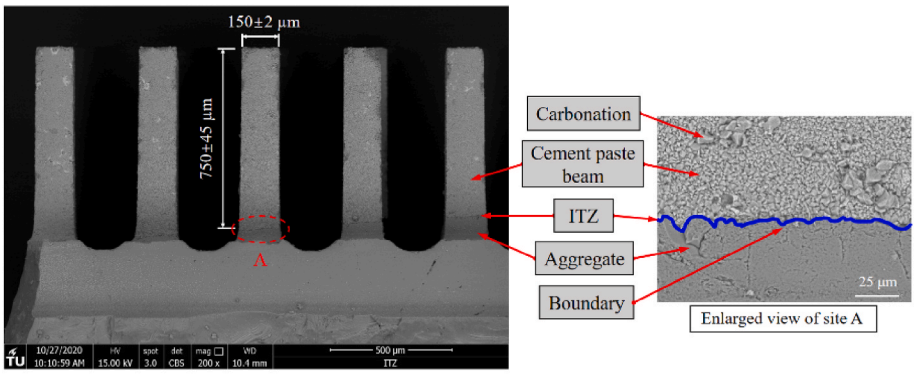

(a)

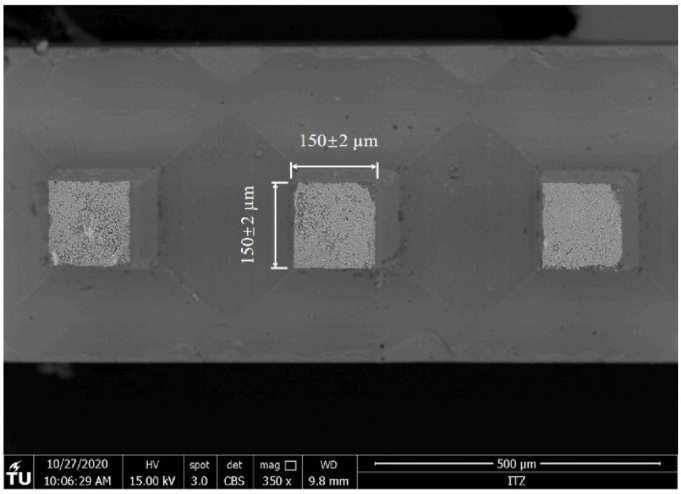

(b)

Fig. 2. Backscattered electron images of (a) the side views and (b) the cross-sections of ITZ samples with w/c 0.4, 28 days.

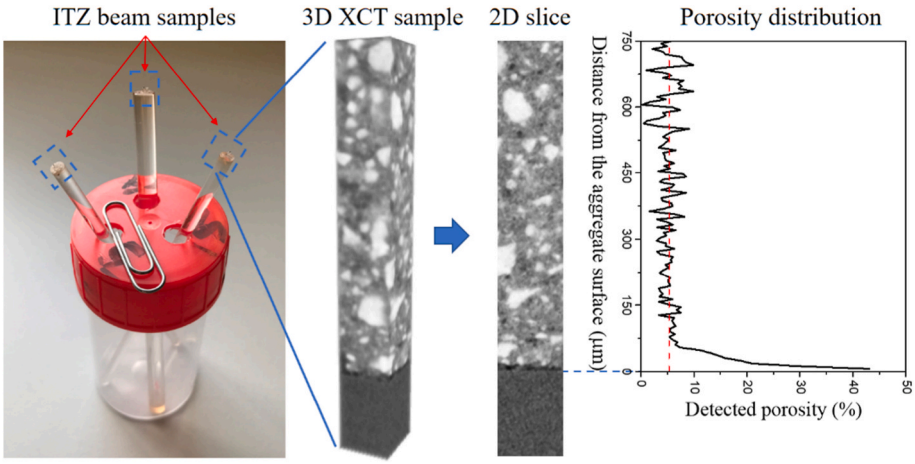

Fig. 3. The 3D XCT results of w/c 0.3 ITZ beam samples and the detected porosity distribution calculated based on segmented 2D slices.

becomes extremely difficult to determine the 'average' effective width of ITZ. Therefore, the exact width of ITZ is not intended to be accurately quantified here.

For demonstration, the region of interest (ROI) with a length of 400 μm cement paste + 100 μm aggregate was extracted from the XCT obtained samples, see Fig. 4. It is found that the changes of porosity in the regions, which are approximately 30–100 μm from the aggregate surface, are most significant. Herein, these regions are roughly considered as the ITZ. It should also be noted that in some cases, the local porosity in ITZ is even similar to the bulk cement paste. As a result of the so-called wall effect [7,8], the unhydrated cement particles tend to be less and smaller in the ITZ. This effect can also be observed in Fig. 4. Due to the limited resolution, other components, such as CH, AFt, and monosulfate (AFm), cannot be distinguished based on the CT images

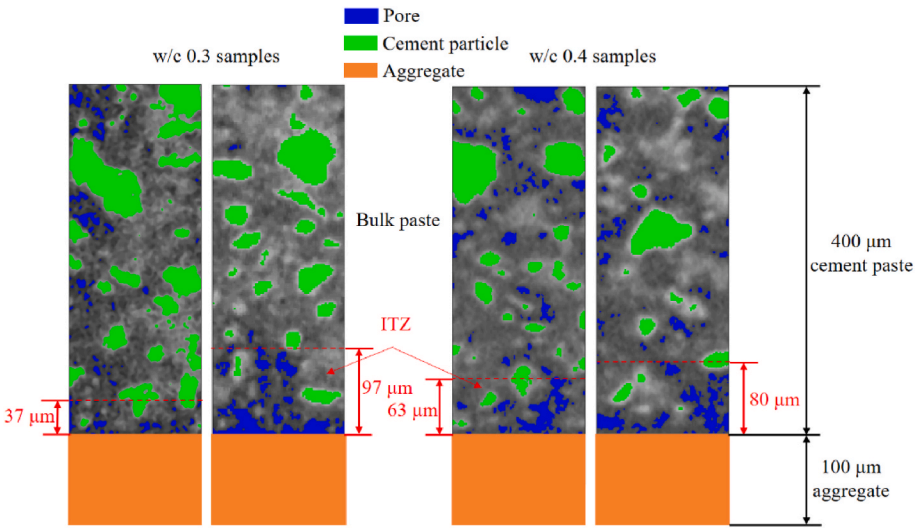

Fig. 4. The segmented pores and unhydrated cement particles in the ROI of two ITZ samples per w/c ratio.

owing to their similar densities as the main hydration products, i.e. C–S–H.

2.2. Quasi-static and fatigue bending test

2.2.1. Experimental set-up

Quasi-static and fatigue bending tests were performed on the fabricated ITZ cantilever beams using the same testing set-up developed in author's previous works [17,38,46,47]. A KLA Nano-indenter G200 equipped with a cylindrical wedge indenter tip was used to apply vertical line loads at the free end of the cantilever beam. Before testing, the angle and centre of the indenter tip were calibrated by probing into a standard aluminum reference sample. One side of aggregate was attached on a metal surface using cyanoacrylate adhesive, and the angle of cement paste beam was carefully adjusted under the in-situ microscope to ensure that the line load is applied perpendicular to the longitudinal axis of the beam. The experimental set-up is schematically shown in Fig. 5. For each test, the coordinates of the loading position and the edge of aggregate surface were recorded under the microscope to determine the loading distance d, see Fig. 5. All tests were conducted in a well-insulated chamber preventing any significant change of temperature and RH. The average temperature and RH during the tests were 26.5 ± 0.5 °C and 34.1% ± 0.8%, respectively. Prior to the tests, the samples were kept in the chamber for temperature equalization until the thermal drift rate was below 0.05 nm/s and the solvent was removed by evaporation.

2.2.2. Quasi-static bending test

The static mechanical properties of ITZ cantilever beams, i.e. flexural strength and static elastic modulus, were determined before performing fatigue tests. For each w/c ratio, 20 cantilever beams were monotonically loaded to failure. The static test was displacement-controlled with a constant loading rate of 50 nm/s. The measured load-displacement curves for two w/c ratios are shown in Fig. 6. Generally, these curves can be divided into two parts: the pre-peak region and the catastrophic failure region. In the pre-peak region, the load increases with the displacement until a critical load is reached. Despite some discontinuities, the pre-peak load-displacement curve is almost linear. Afterwards, a rapid burst of displacement is observed due to the catastrophic failure of the specimen. This is probably because that the nanoindenter is not fast enough to capture the post-peak behaviour of the specimen and the ITZ sample is intrinsically brittle.

In order to determine the flexural strength f_t and static elastic modulus E_{static} of the ITZ sample, the maximum static load P_{max} and the loading slope of load-displacement curve k (in the loading range between 40% and 60% of the maximum load) are respectively used according to the classical beam theory [17,38,48]:

$$f_t = \frac{P_{max} dh}{2I} \tag{1}$$

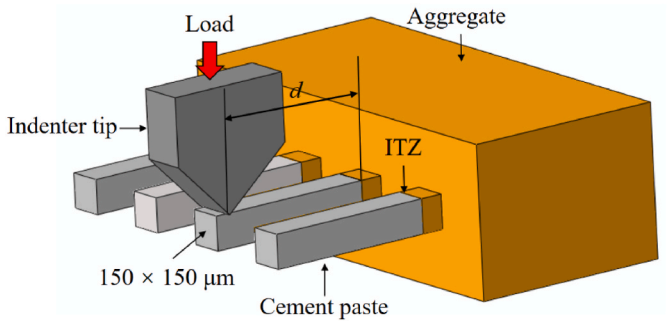

Fig. 5. Schematic diagram of test set-up.

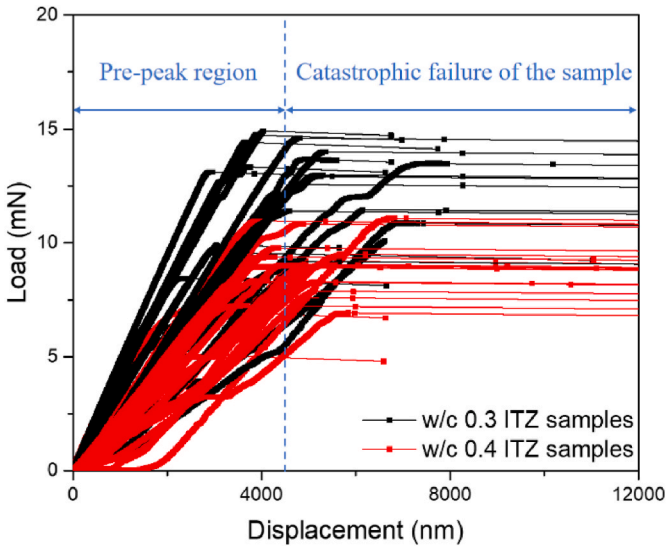

Fig. 6. Load-displacement curves for ITZ samples with two w/c ratios.

$$E_{static} = \frac{kd^3}{3I} \quad (2)$$

where d is the measured effective cantilever length, h is the side length of the square beam cross-section, and $I = h^4/12$ is the moment of inertia. Note that only the linear portion of the load-displacement curve is used to determine the elastic modulus. After the failure of the sample, the fracture location is examined to check whether the fracture occurs at the ITZ region. The fractured surfaces of specimens on the aggregate side were also examined using the scanning electron microscope.

2.2.3. Fatigue bending test

Fatigue flexural tests of ITZ samples were carried out under load control. In total 15 ITZ specimens for each w/c ratio were tested under different cyclic loading ranges (maximum fatigue force F_{max} and minimum force F_{min}). The cyclic load was applied with a constant amplitude (F_{max} - F_{min}) at a loading frequency of 0.55 Hz. The loading protocol is schematically shown in Fig. 7. The pattern of cyclic loading controlled by the nano-indenter is similar to the triangular load but with a very short dwelling time (0.2 s) at the maximum and minimum loads. The corresponding maximum stress at the interface of ITZ sample under the maximum fatigue force was calculated using Eq. (1). Note that even under the same magnitude of the load the calculated stress may be different due to the small variation of the effective cantilever length. The corrected maximum stress level S (σ_{max}/f_t) for the fatigue test varies between 60% and 90% of the static flexural strength for both w/c ratios. At the same time, the minimum stress level for fatigue stress ratio R ($\sigma_{min}/\sigma_{max}$) was maintained at a constant level of 0.07 throughout the test. The number of loading cycles at failure of the specimen was recorded as the fatigue life, N. During the fast loading-unloading regime, small disturbances (2–5% of loading amplitude) for both maximum and minimum fatigue load may occur. Therefore, the recorded average load level was used to determine the stress level. Before each fatigue test, the ITZ sample was preloaded to the maximum load and completely unloaded to reduce the possible plastic deformation generated under the indenter tip [5].

Due to the limited test duration in the used nano-indenter, the fatigue loading protocol was separated into multiple cycle blocks with identical load history. Each cycle block contains 500 loading-unloading cycles. Two cycle blocks are connected in succession with a short rest period (around several minutes), see Fig. 7. The beam is completely unloaded after finishing one cycle block and then reloaded for the next cycle block, as is shown in Fig. 8. The so-called run-out tests are stopped at the limit of 200,000 cycles. At the end of each fatigue test, the nano-indenter will apply a constant low load at around 0.01% of the maximum load to measure the drift rate and calibrate the displacement responses. However, most of the measured drift may be affected by the creep recovery because of the viscoelastic nature of cement paste [49]. Therefore, the calculated drifts were deducted from the total time-dependent displacements.

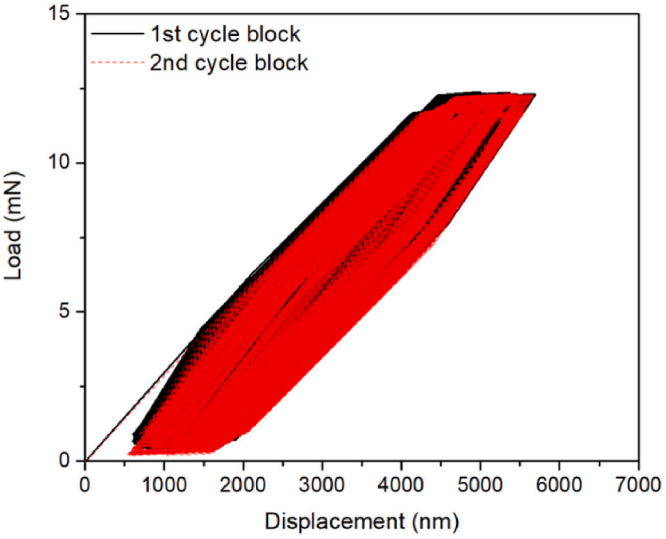

Fig. 8. Examples of load-displacement curves for two cycle blocks.

Two major characters of fatigue of cementitious materials are the evolutions of residual deformation and sample stiffness [5]. A MATLAB code was developed to extract both quantities from the recorded load-displacement curve in each cycle block. Fig. 9 illustrates the calculation of residual deformation and loading stiffness during the fatigue test. The load amplitude and the displacement during the loading stage δ_{load} were used to determine the stiffness of sample at the i-th cycle. The residual displacement δ_{res} is defined as the change of displacement at the maximum load level relative to the corresponding displacement at the first cycle. The corresponding residual strain is calculated as the strain $\varepsilon(t)$ at the upper fibre of the fixed end based on the classical beam theory [48]. The fatigue compliance $C(t)$ is determined by dividing the residual strain by the half of the applied maximum stress ($\sigma_{max}/2$). For each ITZ specimen, the residual strain and the corresponding fatigue compliance were calculated as:

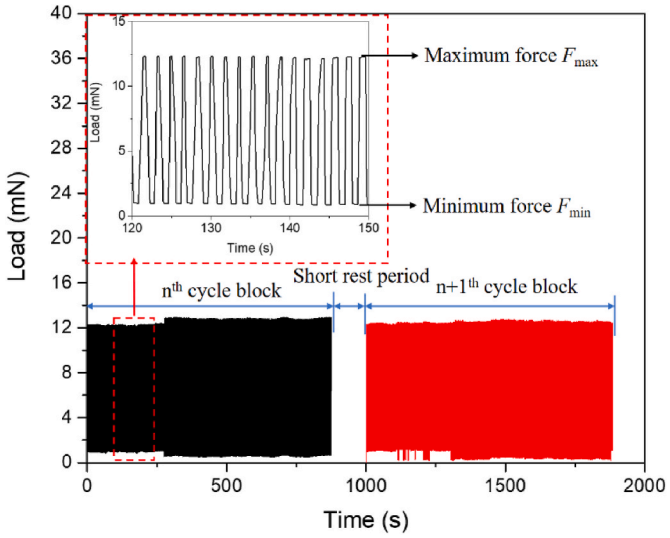

Fig. 7. Illustration of cyclic load history applied in MCB fatigue tests.

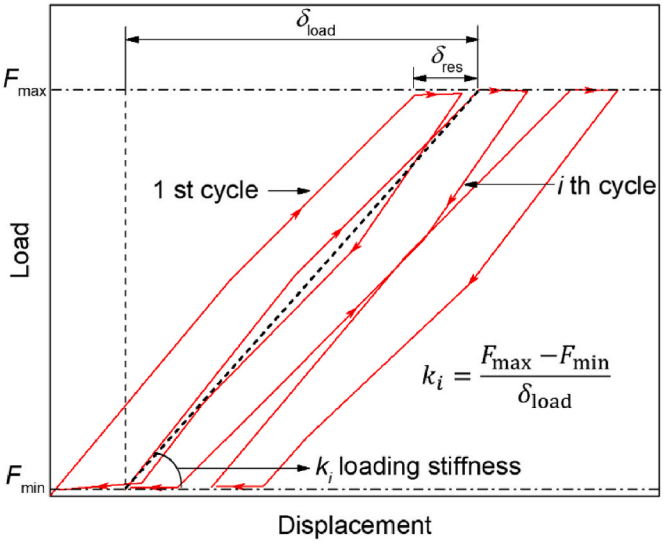

Fig. 9. Illustration of residual displacement and loading stiffness calculation.

$$\varepsilon(t) = \frac{3\delta h}{2L^2} \tag{3}$$

$$C(t) = \frac{2\varepsilon(t)}{\sigma_{max}} \tag{4}$$

where δ is the measured displacement of the indenter tip.

3. Results and discussion

3.1. Mechanical properties

Fig. 10 shows the calculated mechanical properties of ITZ samples. In general, the mechanical properties increase with the decreasing w/c ratio. For comparison, flexural strengths and elastic moduli of cantilever beams made of pure cement paste (28 days) at similar length scale (300 × 300 × 1650 μm^3) [46] are also presented in Fig. 10. As is expected, the mechanical properties of ITZ samples are lower than the pure cement paste samples mainly due to the higher local porosity. The average flexural strength of ITZ samples for both w/c ratios is approximately 44–50% of the paste matrix, while the elastic modulus is around 40–41%. However, there are large variations of flexural strength and elastic modulus indicated by the calculated coefficient of variation i.e. 21-25% for both w/c ratios. Moreover, it is clear that the average flexural strength of the microscopic ITZ specimen is significantly higher than the bonding strength (0.75–3.9 MPa) of macroscopic laboratory-scale specimens [9,10,50]. This aspect is further discussed in Section 3.3.

3.2. Fracture surface

In general, the fracture occurs at the ITZ of the specimen regardless of the loading protocol, i.e. both in static and fatigue conditions. Fig. 11 (a) and (b) show the front and side views of several fractured surfaces of ITZ specimens under monotonic and cyclic loading, respectively. No apparent difference between the static and fatigue fractures is found in this study. It should also be noted that the fracture surface might be different case-by-case in consideration of the high heterogeneity of ITZ. One common characteristic for some fracture surfaces is that the cement paste beam including the ITZ is completely detached from the aggregate surface except for a few remaining cement paste debris. This indicates that the major part of the critical crack is formed along the edge of aggregate and a small portion of the cracking path penetrates into the ITZ. This failure mode is mainly caused by the weak bond between hydration products and the aggregate. Moreover, another failure mode is also observed in some fractured beams, as is shown in Fig. 12(a). In this case, the major part of the critical crack passes through the porous ITZ and exposes a lot of debris on the aggregate surface. The debris mainly consist of amorphous C–S–H gel, CH crystals and some calcium carbonate ($CaCO_3$) cubes formed after the air exposure of the fractured surface. In addition, some minor ettringite (AFt) needles are detected on the aggregate surface. It can be seen in Fig. 12(a) that some large CH crystals (around 10–40 μm) with preferential orientations are anchored in the aggregate surface and surrounded by other hydration products. Similar observations have also been reported in Refs. [8,51]. Note that the preferential orientation of large CH crystal plates may behave in different manners for direct tensile and flexural tests.

It is suggested by several researchers [8,27] that the epitaxial growth of hydration products (e.g. CH and AFt) and their precipitation in small cavities on the aggregate surface, e.g. Fig. 12(b), contribute to the mechanical interlocking effect. This mechanical interlocking effect can be observed at different length scales depending on the roughness of the aggregate surface. Fig. 12(c) illustrates the microscopic mechanical interlocking effect on the ground aggregate surface. Even though the aggregate has been ground to a certain extent, there are still numerous cavities remained on the surface and facilitating the deposition of hydration products. Zimbelmann [10] suggested that the transfer of load from the cement paste to the aggregate is mainly done by the anchored CH crystals and, to a smaller part, by the AFt and C–S–H. It is also believed that large CH crystals formed in the highly porous ITZ would favour the formation and propagation of microcracks under mechanical load [52,53]. It is clear that the ITZ contains excess CH compared to the bulk paste, but the distribution of CH is not a continuous layer around the aggregate surface especially in real concrete samples [8]. This highly heterogeneous microstructure further complicates the fracture behaviour of ITZ at the microscale.

Besides this mechanical effect, the relatively weak electrostatic interaction could also play a role in developing the bond strength [54,55]. According to the zeta-potential measurements and microscopic observations, Ouyang et al. [54] suggested that the adhesion mechanism between C–S–H and silicate filler is driven by an attractive ion-ion correlation force. Since the C–S–H and silicate particles have similar surface charge properties, the electric interaction between the C–S–H surface and silicate surface is similar to that between two C–S–H surfaces. The ion-ion correlations between C–S–H particles have been confirmed in the molecular simulation studies and direct-force measurements by atomic force microscopy [56,57]. The authors [54] suggested that two surfaces (silica and C–S–H) are separated by a dielectric continuum, in which Ca^{2+} ions are free to move. The attractive ion-ion correlation force is generated due to the charges of the excess of Ca^{2+} ions on one side resulting in an overall positive charge, and the deficit on the other side resulting in an overall negative charge. It can be seen in Fig. 12(b) that many C–S–H particles directly precipitate on the aggregate surface. However, this electric interaction effect on the bonding strength seems to also vary largely depending on the distribution of hydration products, especially considering the deposition of other crystal phases on the aggregate surface. Therefore, there are different failure modes, i.e. direct separation or mixed failures between the

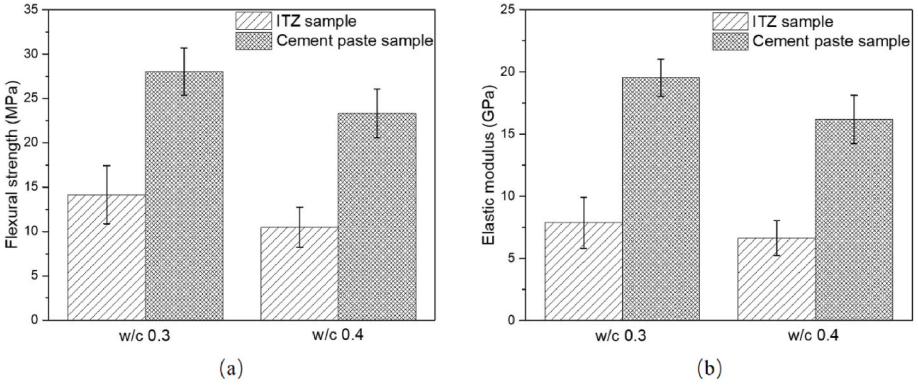

Fig. 10. The comparison of (a) the flexural strength and (b) elastic modulus of ITZ sample (28 d) and the cement paste sample obtained in Ref. [38].

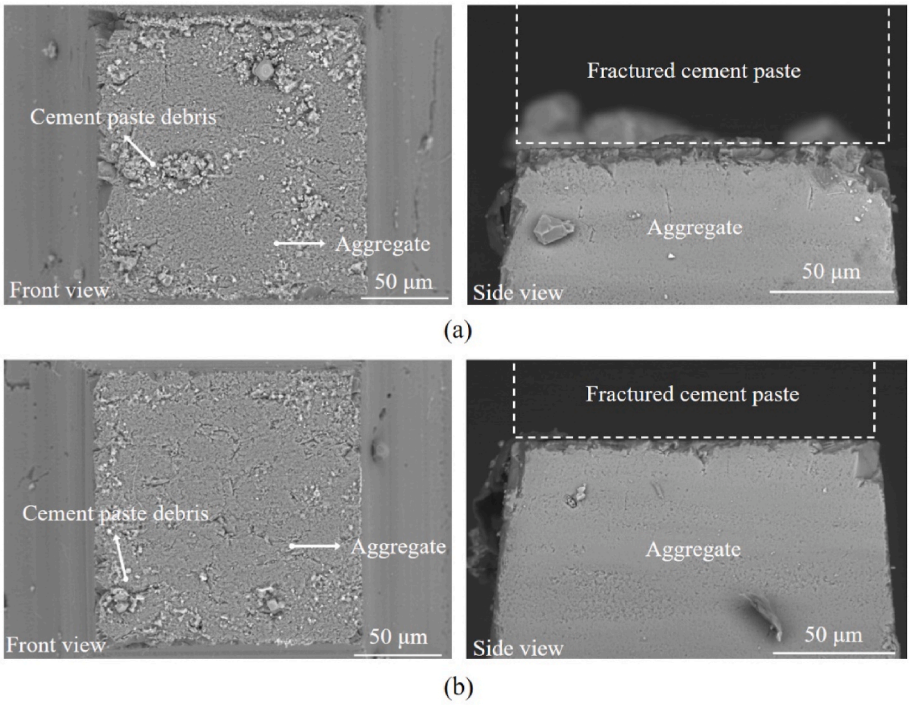

Fig. 11. The front views and side views of fractured ITZ samples subjected to (a) monotonic loading and (b) cyclic loading.

aggregate surface and paste matrix, observed in Figs. 11 and 12, which largely depend on the local microstructure of ITZ. More researches are recommended to assess the adhesion between the aggregate surface with other phases in ITZ [58] and also their fatigue responses.

3.3. Fatigue life

The relationship between the fatigue life N of ITZ specimen and the stress level S is plotted in Fig. 13. For comparison, the fatigue results of cement paste beams [5] were also included. It can be seen that the fatigue life data exhibit a considerable scatter, which is very typical for fatigue tests [59]. Consequently, a clear trend for the S–N relation is difficult to be discerned for any of the investigated w/c ratios. The fatigue resistance of w/c 0.3 specimens is slightly higher than that of w/c 0.4 specimens. but the overall difference in the fatigue strength between the two w/c ratios is not evident. Note that if the fatigue life is plotted against the applied stress magnitude, the fatigue resistance of ITZ specimen with the w/c 0.3 is definitely higher than that of w/c 0.4 specimen. This is because that the static strength of ITZ increases with the decreasing of w/c ratio. The observed scatter of fatigue results may arise from the microstructural heterogeneity of the material, the variation in specimen size, as well as the simplified assumptions made in the fatigue analysis [5]. During most of the fatigue life, the fatigue fracture is characterized by the diffuse microcracking. Instead of instantly turning to the localization of microcracking, the fatigue microcracks gradually propagate at numerous randomly distributed weak spots, e.g. pores and pre-existing cracks [18]. Therefore, the final fatigue fracture depends on a series of time-dependent processes during the loading and unloading cycles. These processes could be related to the stress redistribution, friction process, shrinkage, self-healing and ageing, etc. This is completely different from the static fracture and could also be the reason for the pronounced scatter observed in fatigue data. Nevertheless, it is clear from Fig. 13 that the fatigue life of ITZ specimens for both w/c ratios is apparently shorter compared to the pure cement paste beams at the microscale. This indicates that the ITZ is more vulnerable to the fatigue loading and is most likely to provide locations promoting the crack propagation in concrete, which is in accordance with the findings in Refs. [20,21]. In general, the whole fatigue life of material comprises two major stages: the crack initiation and propagation. Therefore, the effect of weak ITZ on the fatigue of concrete can be twofold: firstly, the lower strength of ITZ and numerous stress concentrations, such as pre-existing cracks generated during the hydration or shrinkage, lead to the instant crack initiation in the ITZ at the early stage of fatigue loading. Secondly, the lower fatigue resistance of ITZ than that of the paste matrix promotes the fatigue crack propagation, resulting in a shorter fatigue life. Moreover, during the re-distribution process under cyclic loading, the stress gradually transfers to the paste matrix, which increases the corresponding stress level. As a result, the fatigue damage evolution in paste matrix is also accelerated. It should be noted that even though the ITZ has significant lower mechanical and fatigue properties compared to the paste matrix, the fatigue damage generated in the ITZ is mostly disconnected depending on the content and distribution of aggregates. The eventual coalescence of fatigue cracks to form the critical crack in concrete depends on the fatigue resistance of paste matrix. In addition, the size effect has been commonly observed in fatigue crack propagation and fatigue life of cement paste and concrete [4,5,60]. However, to the best of the authors' knowledge, there is currently no available data for the direct fatigue testing of the ITZ, either at microscale or macroscale. Therefore, the possible size effect on the fatigue of ITZ cannot be verified here. Besides, caution should be taken to the contribution of aggregate roughness at different length scales [34] to the size-dependent mechanical and fatigue properties of ITZ. For instance, the macroscopic roughness may be related to the manufacturing process, transportation during weathering, etc., on a millimetric observation scale, while the microscopic roughness may be linked to an individual crystal size of the aggregate, on a micrometric observation scale. Apparently, the surface roughness of aggregate at both scales can significantly affect the strength and fatigue properties of ITZ and requires additional research.

3.4. Residual deformation

The measured residual displacement evolution curves for different w/c ratio specimens are shown in Fig. 14. There are large variations in

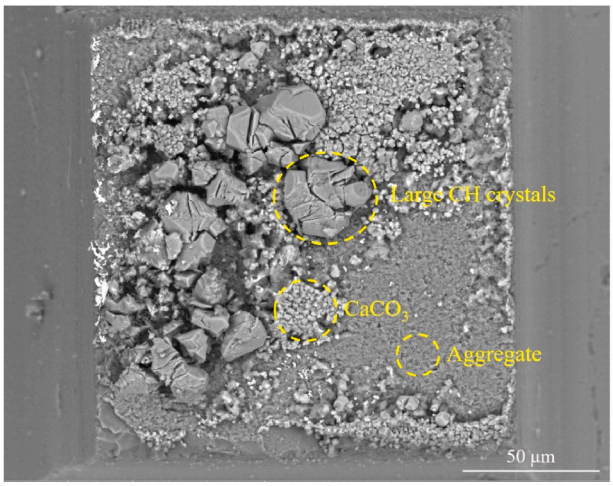

(a)

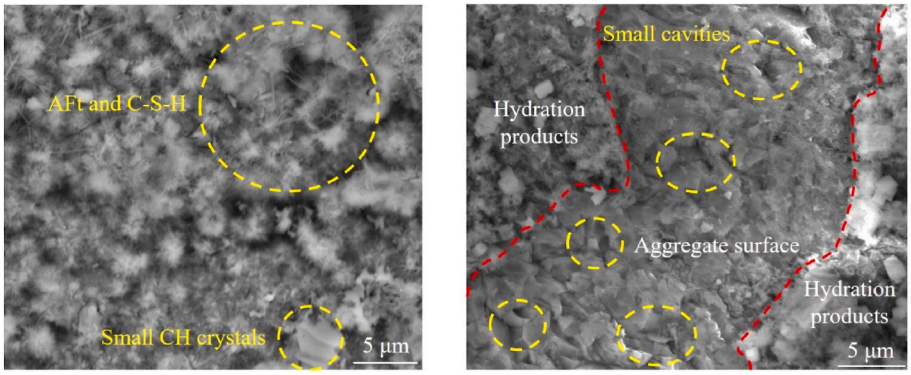

(b)

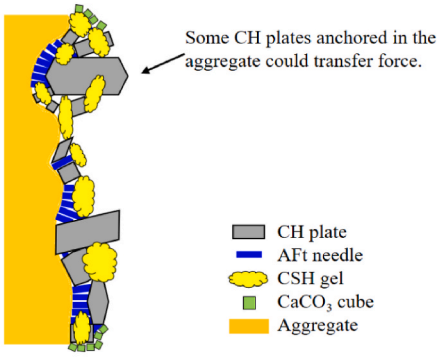

(c)

Fig. 12. (a) Some large CH crystals with preferred orientation observed on the aggregate surface after static fracture; (b) the images of hydration products and small cavities at higher magnifications and (c) schematic presentation of the hydration products distribution on the aggregate surface (Note that the sketch is used for illustration purposes only and the shape and sizes of hydration products are not exact).

the evolution curves mainly due to the microstructural heterogeneity. In general, the curves can be divided into two stages: the initial stage and the stable stage. In the initial stage, the residual deformation increases with a decreasing rate and then reaches to the second stable stage with a constant growth rate. Before the fatigue failure, the evolution curves increase sharply within a few cycles. The fatigue compliance evolutions in the first two stages are calculated based on Equation (4) and shown in Fig. 15. The average fatigue compliance seems to increase with the increasing w/c ratio. It is suggested that the residual deformation in cement paste is mainly caused by the fatigue crack growth as well as the viscoelastic nature of C–S–H [5]. By increasing the w/c ratio, the porosity and the potential of drying shrinkage-induced cracking also increase [61]. Therefore, the fatigue crack growth of the pre-existing microcrack as well as the creep deformation increase in higher w/c ratio ITZ and cement paste samples [20,44]. A comparison of the fatigue compliance evolution between the ITZ and cement paste test results is also presented in Fig. 15. It appears that for the same w/c ratio (0.4), the fatigue compliance of the ITZ specimen is slightly higher than that of pure cement paste specimen, which could be mainly explained by the increased local porosity and microcracking density. Note that the viscoelastic deformation may be affected by the excess amount of non-creeping CH crystals in the local area of ITZ specimens [38]. These two deformation mechanisms observed in fatigue tests are very complicated and, therefore, they are always treated separately without

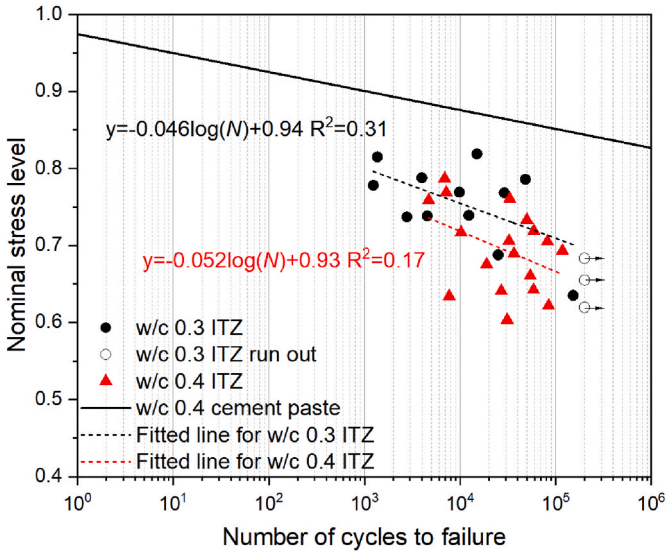

Fig. 13. The S–N curves for ITZ samples and the comparison with the results of pure cement paste samples.

considering their coupled effects [18,62]. Neville and Hirst [63] indicated that the cyclic creep can be considered as an accelerated and irrecoverable static creep. The acceleration effect is explained using Ruetz's model [64] that the applied cyclic stress would disrupt the movement of the adsorbed water layer in C–S–H gel and thus promote the creep deformation. However, the creep effect on the fatigue cracking behaviour is still not clearly understood and should be further investigated.

3.5. Loading stiffness variation

The normalized loading stiffness evolutions of ITZ specimens are also examined and presented in Fig. 16 and Fig. 17. It can be seen in Fig. 16 that the change of loading stiffness is small and the general decreasing trends observed for both w/c ratios are not obvious. However, at the final cycle block of the test, see Fig. 17, the loading stiffness of beam decreased fast in a few cycles before failure. It is worth mentioning that in some fatigue tests the loading stiffness was almost constant and even some slight increases were also observed. Similar observations have also been reported in literature [65,66]. This may indicate some possible strengthening mechanisms during the fatigue tests, such as the carbonation [41], consolidation or compaction of cement paste or the relief of eigenstress in the regions surrounding the cracks under cyclic loading [67]. The stiffness reduction of ITZ specimens at the microscale seems to be slow and limited, which is similar to the findings for cement pastes in Ref. [5]. When a critical crack is formed as a result of the propagation and coalescence of multiple nano-scale cracks, the sudden fatigue failure would occur. In comparison to the pure cement paste specimens, the extent of damage needed for fatigue failure is much less in ITZ specimens as indicated by the lower fatigue strength (Fig. 13). Due to the higher porosity and density of microcracking in ITZ samples, the formation and propagation of the critical fatigue crack would be easier.

3.6. General discussion

It is well known that the strength of quasi-brittle materials is size-dependent [68]. The strength of the ITZ (10.49–14.15 MPa) obtained in this study is significantly higher than the bond strengths measured in conventional laboratory-scale samples using polished aggregate. For instance, Hsu and Slate [69] found that the bond strengths between polished aggregates (sandstone and granite) and cement pastes (w/c 0.265–0.36, age 30 d) were only 1.54–2.39 MPa, which is about 40–61%

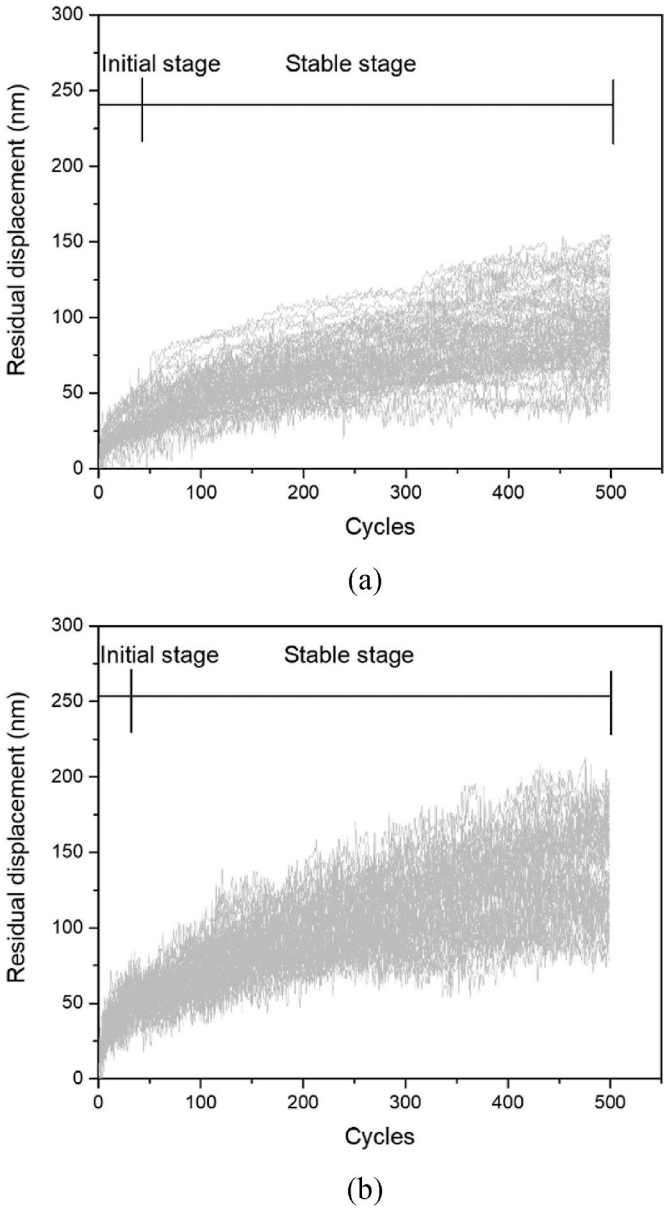

Fig. 14. The evolution curves of residual displacement for (a) w/c 0.3 and (b) w/c 0.4 ITZ specimens.

of the tensile strength of cement matrix. Similar results have also been found in the work of Jebli et al. [11], in which the bond strength (around 1.6 MPa) is around 60% of the strength of bulk paste (w/c 0.5, age 28 d). A relatively high tensile bond strength of around 2.3–3.9 MPa between ground quartzite aggregate surface (with an arithmetic mean height of a line R_a = 3.0 μm) and cement paste (w/c 0.37, age 26–28 d) has also been found in the experimental study conducted by Tasong et al. [9,13]. Furthermore, the authors [9,13] also tested the bond strength of ITZ specimen using much higher surface roughness aggregates (e.g. fractured surfaces with R_a equals to 103.8 μm), which is around 3.25 MPa. However, Zimbelmann [10] observed a much lower bond strength (around 0.75 MPa) between the polished quartz and the cement paste (w/c 0.35, age 28 d), which is only 16% of the tensile strength of bulk paste. Gu et al. [70] also examined the bond strength between the aggregate and mortar (w/c 0.4) using similar surface roughness (R_a = 2.3–4.7 μm) and found that the bond strength is around 1.9 MPa. It is worth mentioning that the strength of ITZ also depends on how the sample is prepared. The shrinkage of the paste, which would introduce eigenstresses in the ITZ [71], could be relieved to a certain extent if the

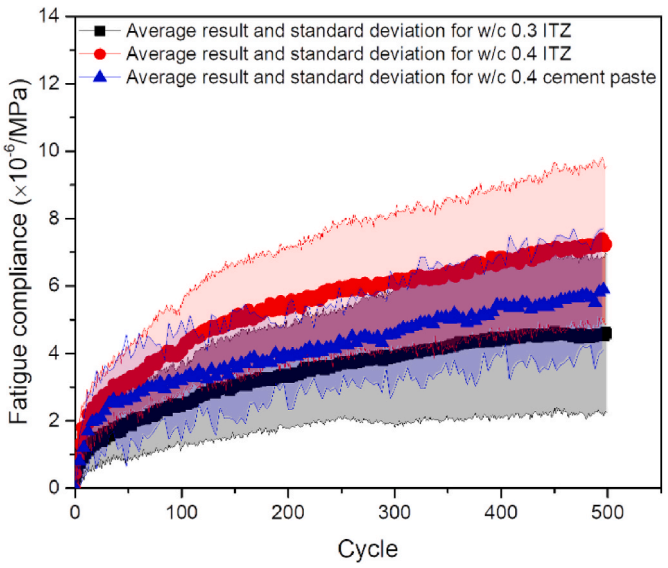

Fig. 15. Comparison of fatigue compliance curves for ITZ and cement paste specimens [5].

ITZ specimen is cut from a larger sample as the way used in this study. Slight different strength may be obtained if the ITZ sample is directly cast in the mold, e.g. in Refs. [9,13,69]. Despite the small differences in the size of macroscopic specimens (i.e. centimeter sized) and mix composition, the bond strength of ITZ reported in the literature is almost one order of magnitude lower than the measured flexural strength of ITZ at the microscale.

It is interesting to note that similar size effect in the splitting strength of cement paste with a wide size range (0.1–40 mm) has also been studied experimentally by Zhang et al. [6]. They found that the average splitting strength of the micro-cube (100 μm) is also one order of magnitude larger than the strength of the laboratory (40 mm) cement paste sample [6]. Even though the compositions and microstructures of ITZ and bulk cement paste are different, they both exhibit similar quasi-brittle fracture behaviour to some extent. Moreover, large capillary pores and air voids that are equivalent to or larger than the dimension of ITZ specimen are completely excluded during the cutting process. Hence, the significantly higher flexural strength of ITZ measured at the microscale seems reasonable.

It is also worth mentioning that the success ratio of preparing the miniaturized ITZ sample is lower than that of pure cement paste sample mainly due to the weak bonding strength. As a result, there could be possible *survival bias* in the measured strength as the remaining samples subjected to the destructive cutting and grinding process would originally exhibit stronger bonding properties, while the weak samples with high local porosities or shrinkage-induced cracks have been eliminated during the sample preparation process. Therefore, the obtained 'average' results may not be fully representative for the true mechanical and fatigue properties. More advanced and nondestructive experimental techniques may be needed. Nevertheless, one should always be careful when interpretating the testing results of ITZ specimens, especially considering the strong microstructural heterogeneity at the microscale.

It is clear that the ITZ is the weakest link in cementitious composites [12]. The much lower strength and lower fatigue resistance of ITZ promote the development of multiple microcracking in concrete samples under monotonic and cyclic loading. To further investigate the effect of local ITZ properties on the macroscopic performance of concrete, it is necessary to employ multiscale modelling approaches. In general, the material structures and local properties of basic components at different length scales need to be considered in the multiscale model [124]. In this way, the material behaviours can be analyzed simultaneously at various scales and the relationship between macroscopic properties and their lower-scale origin can be established. The experimentally measured ITZ properties in this study can, therefore, be used as a benchmark to calibrate and validate interfacial properties in the microscopic model, which serve as an important basis for the multiscale modelling scheme [18,72]. Afterwards, by using appropriate upscaling techniques, the simulated properties of cement paste from the microscopic models can be transferred into the input properties for the mesoscopic model. In

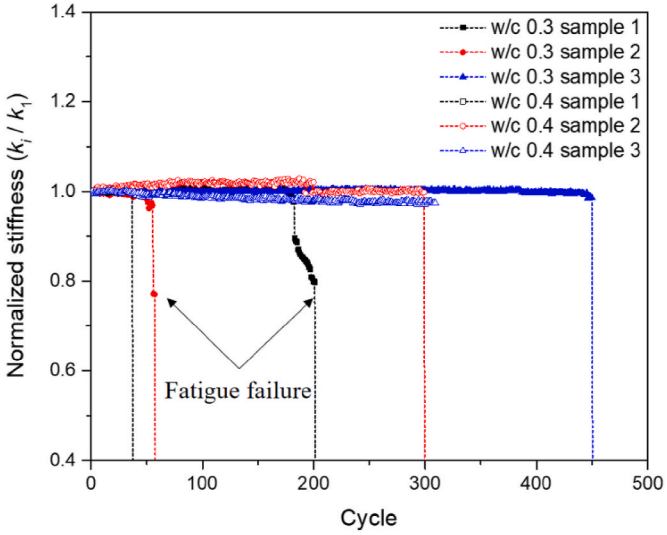

Fig. 17. Normalized stiffness evolution at the final cycle block.

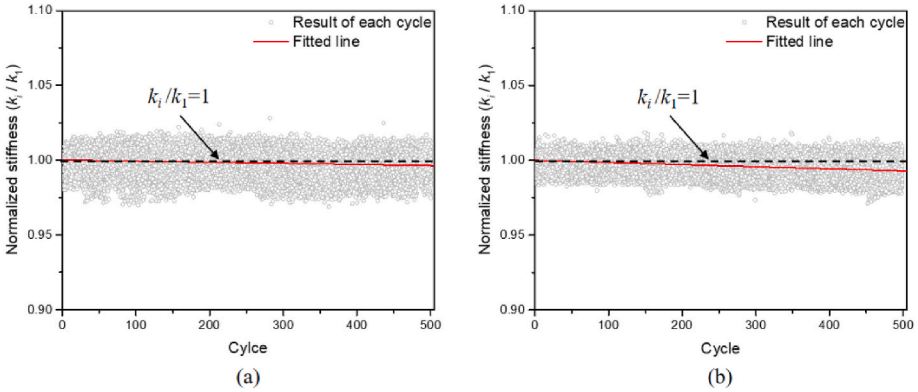

Fig. 16. The evolutions of normalized stiffness during multiple cycle blocks for (a) w/c 0.3 ITZ samples, and (b) w/c 0.4 ITZ samples. Note that the k_1 is the loading stiffness of the first cycle in a cycle block and k_i is the i-th cycle loading stiffness.

addition, all mesoscopic features, such as aggregate shape, ITZ and paste matrix properties, should also be considered in mesoscopic model to provide a reliable quantitative prediction of macroscopic performance of concrete.

4. Conclusions

In this study, the flexural mechanical and fatigue properties of ITZ were investigated at the micrometre length scale using micro-cantilever ITZ specimens. The size effect of ITZ strength was confirmed in current study. The strength of ITZ at the micrometre length scale is almost one order of magnitude higher than that of centimeter sized specimens reported in macroscopic tests. In addition, the measured mechanical properties of ITZ, i.e. the strength and stiffness, are much lower than that of bulk cement paste at similar length scale. The strength of ITZ is around 44–50% of the cement paste, while the elastic modulus is around 40–41%.

The origin of the bond strength between siliceous aggregate and cement paste is discussed. From experimental results it is inferred that the mechanical interlocking at different length scales helps to transfer load. Besides, the electrostatic interaction effect suggested in Ref. [54] also plays a role in contributing the bond strength.

S–N curves for ITZ specimens with two w/c ratios at the microscale were established for the first time. For a given stress level, the fatigue life of w/c 0.3 specimens is slightly longer than that of w/c 0.4 specimens. A lower fatigue resistance was also observed for ITZ compared to the bulk cement paste at the same length scale. However, the results of stiffness variation indicate that very slow and limited fatigue damage was generated in ITZ specimens even before fatigue failure. In addition, relatively higher fatigue residual deformation has also been observed in ITZ tests compared to in tests of cement pastes with the same w/c ratios and ages. The complex residual deformation development is believed to be caused by the combination effect of creep and fatigue crack propagation.

Both the static and fatigue properties of ITZ investigated at the microscale are useful in the validation of microscopic model, which can be further used in the multiscale modelling scheme to predict the fracture behaviour of concrete at the macroscale.

Declaration of competing interest

The authors declare that they have no known competing financial interests or personal relationships that could have appeared to influence the work reported in this paper.

Acknowledgments

Yidong Gan, Minfei Liang and Yu Zhang would like to acknowledge the funding supported by China Scholarship Council under grant number 201706130140, 202007000027 and 201808320456. Hongzhi Zhang acknowledges the financial support from the Taishan Scholar Foundation of Shandong Province under the grant number tsqn201909032 and Natural Science Foundation of Jiangsu Province under grant number of BK20200235 and National Natural Science Foundation of China (52008234). Mr. Arjan Thijssen is also gratefully acknowledged for his help with the ESEM and XCT experiments. The authors would also like to thank Mr. Ameya Kamat for his help with the roughness measurement using the digital microscope.

References

[1] K.M. Simon, J.M. Chandra Kishen, A multiscale approach for modeling fatigue crack growth in concrete, Int. J. Fatig. 98 (2017) 1–13.
[2] C. Pichler, R. Lackner, Identification of logarithmic-type creep of calcium-silicate-hydrates by means of nanoindentation, Strain 45 (2009) 17–25.
[3] J. Zhang, V.C. Li, H. Stang, Size effect on fatigue in bending of concrete, J. Mater. Civ. Eng. 13 (2001) 446–453.
[4] Z.P. Bazant, K. Xu, Size effect in fatigue fracture of concrete, ACI Mater. J. 88 (1991) 390–399.
[5] Y. Gan, H. Zhang, Y. Zhang, Y. Xu, E. Schlangen, K. van Breugel, B. Šavija, Experimental study of flexural fatigue behaviour of cement paste at the microscale, Int. J. Fatig. 151 (2021).
[6] H. Zhang, B. Savija, Y. Xu, E. Schlangen, Size effect on splitting strength of hardened cement paste: experimental and numerical study, Cem. Concr. Compos. 94 (2018) 264–276.
[7] K.L. Scrivener, A.K. Crumbie, P. Laugesen, The interfacial transition zone (ITZ) between cement paste and aggregate in concrete, Interface Sci. 12 (2004) 411–421.
[8] S. Diamond, J. Huang, The ITZ in concrete - a different view based on image analysis and SEM observations, Cem. Concr. Compos. 23 (2001) 179–188.
[9] W.A. Tasong, C.J. Lynsdale, J.C. Cripps, Aggregate-cement paste interface Part I. Influence of aggregate geochemistry, Cement Concr. Res. 28 (1998) 1453–1465.
[10] R. Zimbelmann, A contribution to the problem of cement-aggregate bond, Cement Concr. Res. 15 (1985) 801–808.
[11] M. Jebli, F. Jamin, E. Malachanne, E. Garcia-Diaz, M.S. El Youssoufi, Experimental characterization of mechanical properties of the cement-aggregate interface in concrete, Construct. Build. Mater. 161 (2018) 16–25.
[12] K. Wu, H. Shi, L. Xu, G. Ye, G. De Schutter, Microstructural characterization of ITZ in blended cement concretes and its relation to transport properties, Cement Concr. Res. 79 (2016) 243–256.
[13] W.A. Tasong, C.J. Lynsdale, J.C. Cripps, Aggregate-cement paste interface. II: influence of aggregate physical properties, Cement Concr. Res. 28 (1998) 1453–1465.
[14] I.F. Sáez del Bosque, W. Zhu, T. Howind, A. Matías, M.I. Sánchez de Rojas, C. Medina, Properties of interfacial transition zones (ITZs) in concrete containing recycled mixed aggregate, Cem. Concr. Compos. 81 (2017) 25–34.
[15] J. Xiao, W. Li, Z. Sun, D.A. Lange, S.P. Shah, Properties of interfacial transition zones in recycled aggregate concrete tested by nanoindentation, Cem. Concr. Compos. 37 (2013) 276–292.
[16] H. Zhang, Y. Gan, Y. Xu, S. Zhang, E. Schlangen, B. Šavija, Experimentally informed fracture modelling of interfacial transition zone at micro-scale, Cem. Concr. Compos. 104 (2019).
[17] Y. Gan, H. Zhang, B. Šavija, E. Schlangen, K. van Breugel, Static and fatigue tests on cementitious cantilever beams using nanoindenter, Micromachines 9 (2018).
[18] Y. Gan, H. Zhang, M. Liang, E. Schlangen, K. van Breugel, B. Šavija, A numerical study of fatigue of hardened cement paste at the microscale, Int. J. Fatig. 151 (2021), 106401.
[19] K. van Breugel, D. Koleva, T. van Beek, The Ageing of Materials and Structures: towards Scientific Solutions for the Ageing of Our Assets, 2017.
[20] A. Toumi, A. Bascoul, A. Turatsinze, Crack propagation in concrete subjected to flexural- cyclic loading, Mater. Struct. 31 (1998) 451–458.
[21] M. Saito, Characteristics of microcracking in concrete under static and repeated tensile loading, Cement Concr. Res. 17 (1987) 211–218.
[22] T.T.C. Hsu, Fatigue of plain concrete, ACI J. Proc. 78 (1981) 292–304.
[23] P. Paris, F. Erdogan, A critical analysis of crack propagation laws, J. Basic Eng. 85 (1963) 528–533.
[24] D. Hordijk, Local Approach to Fatigue of Concrete, PhD Thesis, Delft Univ. Technol., 1991, p. 216.
[25] K.M.P. Fathima, J.M.C. Kishen, A thermodynamic framework for the evolution of damage in concrete under fatigue, Arch. Appl. Mech. 85 (2015) 921–936.
[26] W. Schütz, A history of fatigue, Eng. Fract. Mech. 54 (1996) 263–300.
[27] V. Slowik, G.A. Plizzari, V.E. Saouma, Fracture of concrete under variable amplitude fatigue loading, ACI Mater. J. 93 (1996) 272–283.
[28] J. Lemaitre, A continuous damage mechanics model for ductile fracture, J. Eng. Mater. Technol. Trans. ASME. 107 (1985) 83–89.
[29] J.L. Chaboche, Anisotropic creep damage in the framework of continuum damage mechanics, Nucl. Eng. Des. 79.3 (1983) 309–319.
[30] F. Leckie, A Course on Damage Mechanics, Springer Science & Business Media, 1998.
[31] W. Suaris, C. Ouyang, V.M. Fernando, Damage model for cyclic loading of concrete, J. Eng. Mech. 116 (1990) 1020–1035.
[32] T. Akçaoğlu, M. Tokyay, T. Çelik, Effect of coarse aggregate size and matrix quality on ITZ and failure behavior of concrete under uniaxial compression, Cem. Concr. Compos. 26 (2004) 633–638.
[33] P.J.M. Monteiro, J.C. Maso, J.P. Ollivier, The aggregate-mortar interface, Cement Concr. Res. 15 (1985) 953–958.
[34] P.H.F. Loz, J.P. Monticelli, M.M. Futai, E. Tutumluer, D.A. Lange, S.C. Angulo, Roughness of natural aggregates by interferometry and its microstructure, Construct. Build. Mater. 297 (2021), 123646.
[35] S. Caliskan, B. Karihaloo, Effect of surface roughness, type and size of model aggregates on the bond strength of aggregate/mortar, Interface Sci. 12 (2004) 361–374.
[36] Y. Gao, G. De Schutter, G. Ye, Z. Tan, K. Wu, The ITZ microstructure, thickness and porosity in blended cementitious composite: effects of curing age, water to binder ratio and aggregate content, Compos. B Eng. 60 (2014) 1–13.
[37] K.L. Scrivener, P.L. Pratt, Quantitative Characterization of the Transition Zone in High Strength Concretes, 1988, p. 1.
[38] Y. Gan, M. Vandamme, H. Zhang, Y. Chen, E. Schlangen, K. van Breugel, B. Šavija, Micro-cantilever testing on the short-term creep behaviour of cement paste at micro-scale, Cement Concr. Res. 134 (2020) 1–26.
[39] H. Zhang, B. Šavija, E. Schlangen, Combined experimental and numerical study on micro-cube indentation splitting test of cement paste, Eng. Fract. Mech. 199 (2018) 773–786.

[40] J. Zhang, G.W. Scherer, Comparison of methods for arresting hydration of cement, Cement Concr. Res. 41 (2011) 1024–1036.
[41] H. Zhang, C.R. Rodriguez, H. Dong, Y. Gan, E. Schlangen, B. Šavija, Elucidating the effect of accelerated carbonation on porosity and mechanical properties of hydrated Portland cement paste using X-ray tomography and advanced micromechanical testing, Micromachines 11 (2020).
[42] M.A. Vicente, D.C. González, J. Mínguez, M.A. Tarifa, G. Ruiz, R. Hindi, Influence of the pore morphology of high strength concrete on its fatigue life, Int. J. Fatig. 112 (2018) 106–116.
[43] H. Zhang, B. Šavija, S.C. Figueiredo, M. Lukovic, E. Schlangen, Microscale testing and modelling of cement paste as basis for multi-scale modelling, Materials 9 (2016).
[44] Y. Gan, C. Romero Rodriguez, H. Zhang, E. Schlangen, K. van Breugel, B. Šavija, Modeling of microstructural effects on the creep of hardened cement paste using an experimentally informed lattice model, Comput. Civ. Infrastruct. Eng. 36 (2021) 560–576.
[45] G. Ye, Experimental Study and Numerical Simulation of the Development of the Microstructure and Permeability of Cementitious Materials, 2003.
[46] Y. Gan, C.R. Rodriguez, E. Schlangen, K. van Breugel, B. Šavija, Assessing strain rate sensitivity of cement paste at the micro-scale through micro-cantilever testing, Cem. Concr. Compos. 121 (2021).
[47] Y. Gan, H. Zhang, B. Šavija, E. Schlangen, K. van Breugel, Micro-cantilever testing of cementitious materials under various loading conditions, Proc. 10th Int. Conf. Fract. Mech. Concr. Concr. Struct. (2019).
[48] G.R. Cowper, The shear coefficient in Timoshenko's beam theory, J. Appl. Mech. 33 (1966) 335.
[49] Y. Gan, M. Vandamme, Y. Chen, E. Schlangen, K. van Breugel, B. Šavija, Experimental investigation of the short-term creep recovery of hardened cement paste at micrometre length scale, Cement Concr. Res. 149 (2021) 106562.
[50] G.A. Rao, B.K.R. Prasad, Influence of the roughness of aggregate surface on the interface bond strength, Cement Concr. Res. 32 (2002) 253–257.
[51] P. Vargas, O. Restrepo-Baena, J.I. Tobón, Microstructural analysis of interfacial transition zone (ITZ) and its impact on the compressive strength of lightweight concretes, Construct. Build. Mater. 137 (2017) 381–389.
[52] G. Prokopski, J. Halbiniak, Interfacial transition zone in cementitious materials, Cement Concr. Res. 30 (2000) 1–5.
[53] K. Liao, P. Chang, Y. Peng, C. Yang, A study on characteristics of interfacial transition zone in concrete, Cement Concr. Res. 34 (2004) 977–989.
[54] X. Ouyang, D.A. Koleva, G. Ye, K. van Breugel, Understanding the adhesion mechanisms between C-S-H and fillers, Cem, Concr. Res. 100 (2017) 275–283.
[55] R.J.M. Pellenq, H. Van Damme, Why does concrete set?: the nature of cohesion forces in hardened cement-based materials, MRS Bull. 29 (2004) 319–323.
[56] A. Gmira, M. Zabat, R.J.M. Pellenq, H. Van Damme, Microscopic physical basis of the poromechanical behavior of cement-based materials, Mater. Struct. Constr. 37 (2004) 3–14.
[57] C. Plassard, E. Lesniewska, I. Pochard, A. Nonat, Nanoscale experimental investigation of particle interactions at the origin of the cohesion of cement, Langmuir 21 (2005) 7263–7270.
[58] L. Armelao, A. Bassan, R. Bertoncello, G. Biscontin, S. Daolio, A. Glisenti, Silica glass interaction with calcium hydroxide: a surface chemistry approach, J. Cult. Herit. 1 (2000) 375–384.
[59] J.J. Ortega, G. Ruiz, R.C. Yu, N. Afanador-García, M. Tarifa, E. Poveda, X. Zhang, F. Evangelista, Number of tests and corresponding error in concrete fatigue, Int. J. Fatig. 116 (2018) 210–219.
[60] K. Kirane, Z.P. Bažant, Size effect in Paris law and fatigue lifetimes for quasibrittle materials: modified theory, experiments and micro-modeling, Int. J. Fatig. 83 (2016) 209–220.
[61] W. Hansen, Drying shrinkage mechanisms in Portland cement paste, J. Am. Ceram. Soc. 70 (1987) 323–328.
[62] Z.P. Bazant, M.H. Hubler, Theory of cyclic creep of concrete based on Paris law for fatigue growth of subcritical microcracks, J. Mech. Phys. Solid. 63 (2014) 187–200.
[63] A.M. Neville, G.A. Hirst, Mechanism of cyclic creep of concrete, Spec. Publ. 55 (1978) 83–102.
[64] W. Ruetz, A hypothesis for the creep of hardened cement paste and the influence of simultaneous shrinkage, Proc. Struct. Concr. Its Behav. under Load (1968) 365–387.
[65] B. Isojeh, M. El-Zeghayar, F.J. Vecchio, Concrete damage under fatigue loading in uniaxial compression, ACI Mater. J. 114 (2017).
[66] M.E. Awad, Strength and Deformation Characteristics of Plain Concrete Subjected to High Repeated and Sustained Loads, University of Illinois Engineering Experiment Station. College of Engineering, University of Illinois at Urbana-Champaign., 1971.
[67] M. Corrado, J.F. Molinari, Effects of residual stresses on the tensile fatigue behavior of concrete, Cement Concr. Res. 89 (2016) 206–219.
[68] Z.P. Bažant, Size effect in blunt fracture: concrete, rock, metal, J. Eng. Mech. 110 (1984) 518–535.
[69] T.T.C. Hsu, F.O. Slate, Tensile bond strength between aggregate and cement paste or mortar, ACI J. Proc. 60 (1963) 465–486.
[70] X. Gu, L. Hong, Z. Wang, F. Lin, Experimental study and application of mechanical properties for the interface between cobblestone aggregate and mortar in concrete, Construct. Build. Mater. 46 (2013) 156–166.
[71] J. Bisschop, P. Lura, J.G.M. Van Mier, Shrinkage microcracking in cement-based materials with low water-cement ratio, Concr. Sci. Eng. 3 (2001) 151–156.
[72] H. Zhang, Y. Xu, Y. Gan, E. Schlangen, B. Šavija, Experimentally validated meso-scale fracture modelling of mortar using output from micromechanical models, Cem. Concr. Compos. 110 (2020).